

The GBT Diffuse Ionized Gas Survey (GDIGS): Discrete Sources

DYLAN J. LINVILLE,^{1,2} MATTEO LUISI,^{2,3} L. D. ANDERSON,^{1,2,4} BIN LIU,^{5,6} T. M. BANIA,⁷ DANA. S. BALSER,⁸
TREY V. WENGER,^{9,10} L. M. HAFFNER,¹¹ AND J. L. MASCOOP^{1,2}

¹*Department of Physics and Astronomy, West Virginia University, Morgantown, WV 26506, USA*

²*Center for Gravitational Waves and Cosmology, West Virginia University, Chestnut Ridge Research Building, Morgantown, WV 26505, USA*

³*Department of Physics, Westminster College, New Wilmington, PA 16172, USA*

⁴*Adjunct Astronomer at the Green Bank Observatory, P.O. Box 2, Green Bank, WV 24944, USA*

⁵*National Astronomical Observatories, Chinese Academy of Sciences, Beijing 100012, China*

⁶*CAS Key Laboratory of FAST, NAOC, Chinese Academy of Sciences, China*

⁷*Institute for Astrophysical Research, Astronomy Department, Boston University, 725 Commonwealth Ave., Boston, MA 02215, USA*

⁸*National Radio Astronomy Observatory, 520 Edgemont Road, Charlottesville, VA 22903, USA*

⁹*Dominion Radio Astrophysical Observatory, Herzberg Astronomy and Astrophysics Research Centre, National Research Council, P.O. Box 248, Penticton, BC V2A 6J9, Canada*

¹⁰*NSF Astronomy & Astrophysics Postdoctoral Fellow, Department of Astronomy, University of Wisconsin-Madison, Madison, WI 53706, USA*

¹¹*Department of Physical Sciences, Embry-Riddle Aeronautical University, Daytona Beach FL 32114, USA*

ABSTRACT

The Green Bank Telescope (GBT) Diffuse Ionized Gas Survey (GDIGS) traces ionized gas in the Galactic midplane by observing radio recombination line (RRL) emission from 4–8 GHz. The nominal survey zone is $32.3^\circ > \ell > -5^\circ$, $|b| < 0.5^\circ$. Here, we analyze GDIGS H α ionized gas emission toward discrete sources. Using GDIGS data, we identify the velocity of 35 H II regions that have multiple detected RRL velocity components. We identify and characterize RRL emission from 88 H II regions that previously lacked measured ionized gas velocities. We also identify and characterize RRL emission from eight locations that appear to be previously-unidentified H II regions and 30 locations of RRL emission that do not appear to be H II regions based on their lack of mid-infrared emission. This latter group may be a compact component of the Galactic Diffuse Ionized Gas (DIG). There are an additional 10 discrete sources that have anomalously high RRL velocities for their locations in the Galactic plane. We compare these objects' RRL data to ¹³CO, HI and mid-infrared data, and find that these sources do not have the expected 24 μ m emission characteristic of H II regions. Based on this comparison we do not think these objects are H II regions, but we are unable to classify them as a known type of object.

Keywords: Warm ionized medium (1788), Interstellar Plasma (851), H II regions (694), Radio continuum emission (1340), Interstellar medium (847)

1. INTRODUCTION

Ionized gas in the plane of the Milky Way can be decomposed into discrete clumps, particularly H II regions, and a diffuse component known as the “Diffuse Ionized Gas” (DIG). H II regions are zones of ionized gas that form around spectral type O and B stars, where the star's immense energy output ionizes the surrounding

medium. These massive stars only live ~ 10 Myr. H II regions are therefore useful indicators of active massive star formation. In contrast to H II regions, the DIG is spread throughout the Galactic disk, has a lower electron density near $n_e \sim 10^{-2} \text{ cm}^{-3}$ (Lyne et al. 1985) compared to densities of $n_e \sim 10^2 \text{ cm}^{-3}$ or greater found in H II regions (Lockman & Brown 1975), and is not typically associated with specific stars.

We can study Galactic ionized gas using transitions of excited hydrogen atoms. Recombination lines are produced after electrons and ions recombine into an excited

state. For nearby plasma, H α line observations such as those made by the Wisconsin H α Mapper (WHAM) survey (Reynolds et al. 1998; Haffner et al. 2003) provides sensitive observations that can determine gas properties. The H α line, although bright, is attenuated by dust and so is of limited use for distant H II regions. Radio recombination lines (RRLs) are less affected by extinction compared to H α and so are the preferred tracer for more distant H II regions and the DIG.

Previous targeted RRL surveys have been instrumental in assembling the catalog of known H II regions. In particular, the H II Region Discovery Survey (HRDS; Anderson et al. 2011a) and Southern H II Region Discovery Survey (SHRDS; Wenger et al. 2021) have more than doubled the number of known H II regions (Anderson et al. 2018a). An ionized gas spectroscopic detection determines the source’s velocity relative to the local standard of rest (LSR). Such pointed observations, however, have an inherent weakness: they are by nature biased toward sources meeting the criteria for inclusion in the study.

Large-scale mapped RRL surveys allow for the study of ionized gas across the Galaxy. The Green Bank Telescope (GBT) Diffuse Ionized Gas Survey (GDIGS) is a RRL survey that was conducted with the goal of studying ionized gas in the Galactic midplane. GDIGS offers several advantages over previous blind RRL surveys in the survey zone. Such surveys lacked the sensitivity and resolution necessary to detect many new discrete sources. The Survey of Ionized Gas in the Galaxy, made with the Arecibo Telescope (SIGGMA), an RRL survey near 1.4 GHz, has a sensitivity of ~ 1 mJy beam $^{-1}$ at 5 km s $^{-1}$ spectral resolution and $\sim 3'.4$ spatial resolution (Liu et al. 2013; Liu et al. 2019). The HI Parkes All Sky Survey (HIPASS) RRL survey, has 6.4 mJy beam $^{-1}$ sensitivity at 20 km s $^{-1}$ spectral resolution and 14'.4 spatial resolution, also near 1.4 GHz (Alves et al. 2015). As detailed subsequently in Section 2, GDIGS improves upon both of these surveys in sensitivity, spatial resolution, and spectral resolution. We can use GDIGS to partially correct for the intrinsic coverage bias of pointed surveys by locating otherwise unidentified sources within the survey zone, $32.3^\circ > \ell > -5^\circ$, $|b| < 0.5^\circ$. GDIGS is a blind survey, and is consequently sensitive to populations that targeted surveys miss. This feature of mapped surveys like GDIGS is especially relevant for studying clumps of the DIG, which the inclusion criteria of targeted surveys ignore. Using mapped surveys to study H II populations has been shown to be effective in Hou et al. (2022). Hou et al. (2022) mapped the Galactic plane in RRL emission near 1 GHz over $55^\circ > \ell > 33^\circ$, $|b| < 2.0^\circ$ with a sensitivity of 0.25 mJy beam $^{-1}$, at

2.2 km s $^{-1}$ spectral resolution and $\sim 3'$ spatial resolution using the Five-hundred-meter Aperture Spherical radio Telescope (FAST). This survey does not overlap with the GDIGS survey area. With GDIGS we are therefore able to obtain a more complete census of H II regions and assorted DIG features in the observed section of the Galactic disk than with previous targeted surveys.

Here we use GDIGS data to investigate new sources of RRL emission and to re-analyze previously known sources in ways that only a blind survey allows. We distinguish the emission from known H II regions using version 2.4 of the WISE Catalog of Galactic H II regions (Anderson et al. 2014, hereafter the “WISE Catalog”). The WISE Catalog is statistically complete for H II regions ionized by O-type stars (Armentrout et al. 2017). One goal with this study is to improve the WISE Catalog by providing RRL detections and associated information, particularly velocity measurements, for as many sources previously lacking such observations as possible within the GDIGS survey area. We also intend to locate any previously unreported H II regions in the survey area. In the course of the study we encountered numerous regions of discrete RRL emission that do not fit the previously described characteristics of H II regions. We report these in Sections 3.2.2 and 3.2.3.

2. DATA

2.1. GDIGS Data

GDIGS is a survey of ionized gas in the midplane of the Milky Way. The GDIGS RRL data were first published in Anderson et al. (2021). A complete description of the details of data collection and processing can be found there, while a shorter summary is provided here.

The GDIGS data were collected using the C-band receiver on the Green Bank Telescope (GBT) in total power mode. Within the 4–8 GHz bandpass, we tuned to 15 usable hydrogen RRLs, as defined in Anderson et al. (2021). The reduced data of average hydrogen RRL emission have a spatial resolution of $2'.65$ and 0.5 km s $^{-1}$ spectral resolution. The rms spectral noise per spaxel is ~ 10 mK, with sensitivity to emission measures $EM \gtrsim 1100$ pc cm $^{-6}$. This emission measure translates to a mean electron density of $\langle n_e \rangle \gtrsim 30$ cm $^{-3}$ for a 1 pc path length, or $\langle n_e \rangle \gtrsim 1$ cm $^{-3}$ for a 1 kpc path length. Our data processing methodology is described in Anderson et al. (2021).

2.2. MIR Data

Mid-infrared (MIR) observations are an important diagnostic tool used to determine if an ionized gas source is an H II region or another class of object. We use 3.6 μ m and 8.0 μ m data from the Spitzer GLIMPSE sur-

vey (Benjamin et al. 2003; Churchwell et al. 2009) and $24\ \mu\text{m}$ data from the MIPS GAL survey (Carey et al. 2009). These surveys provide the best resolution and sensitivity available. H II regions have strong emission at these wavelengths, particularly $8.0\ \mu\text{m}$ and $24\ \mu\text{m}$.

2.3. The WISE Catalog

We compare the regions discussed in this paper to those of the WISE Catalog. The WISE Catalog is the largest, most complete catalog of Galactic H II regions, and contains all 8416 known H II regions and H II region candidates. The catalog distinguishes H II regions from other ionized gas sources by their characteristic emission.

There are four types of sources listed in the catalog: “known,” “candidate,” “group,” and “radio quiet.” Known sources have detected spectroscopic ionized gas emission as well as $\sim 20\ \mu\text{m}$ emission. Candidate sources have radio continuum emission coincident with their $\sim 20\ \mu\text{m}$ emission and are thus likely to be real H II regions, but do not have a spectroscopic ionized gas detection. Radio quiet sources have MIR emission but lack associated radio continuum emission; this may be because the radio continuum emission is too faint, or because existing surveys do not cover the sources. Finally, group sources are located nearby “Known” H II regions and are thought to be part of a larger complex but do not have measured spectroscopic ionized gas emission. The latter three of these categories— “candidate”, “group”, and “radio quiet” sources- are suspected to be H II regions but require confirmation before they can be moved to the “known” category. The detection of RRL emission from WISE Catalog sources previously lacking such a detection provides both confirmation that the source is an H II region and also an LSR velocity that can be used to derive a kinematic distance. We use the presence of these tracers in our identification of new regions below.

The census of H II regions in the WISE Catalog is lacking information for a large fraction of its 8416 entries, ~ 2000 of which fall within the GDIGS survey area. Many objects have multiple reported ionized gas velocity components and therefore lack a unique LSR velocity assignment, which is a requirement for calculating a kinematic distance. There are 2361 confirmed H II regions with spectroscopic gas detections. The WISE Catalog lacks spectroscopic gas detection for 72% of its entries, including 626 “group” H II regions, 1681 H II region candidates, and 3748 radio-quiet H II region candidates.

3. GDIGS DISCRETE SOURCES

GDIGS is a blind survey of ionized gas in the Galactic plane and is therefore a useful dataset both for characterizing previously-known H II regions and for searching

for other discrete sources of ionized gas. We examine GDIGS RRL emission from sources in the WISE Catalog to determine the velocity of the source and, where applicable, to confirm that the source is an H II region. We also search the GDIGS survey data for new H II regions that do not appear in the WISE Catalog, and locate numerous locations of compact RRL emission that lack MIR emission.

3.1. WISE Catalog Objects

We explore detections in the GDIGS survey data of sources belonging to the WISE Catalog. Due to confusion within the GDIGS beam, we are only able to conclusively associate GDIGS emission with WISE Catalog sources that are isolated or are angularly large. Smaller, more tightly grouped regions are likely to be indistinguishable from each other at the GDIGS spatial resolution.

Some WISE Catalog sources are in close angular proximity with each other and share the same reported velocity or velocities. In these cases both objects were originally observed in the same telescope beam. Following the methodology used to construct the WISE Catalog, we report the same measured velocities for both objects.

3.1.1. Multiple-Velocity H II Regions

Many previously-known H II regions have more than one measured RRL emission velocity component, which complicates efforts to calculate the regions’ kinematic distances and other physical parameters. In the HRDS, for instance, over 30% of all detected H II regions have more than one RRL velocity (Anderson et al. 2015a). For such regions, one velocity component presumably comes from the H II region itself, and the other component(s) from the DIG along the line of sight. We are confident in this assumption because two H II regions along a single line of sight is statistically unlikely (Anderson et al. 2015a). With their large beams and sensitivity to extended emission, single-dish observations are especially susceptible to detecting emission from diffuse RRL emission in the same pointing.

Many sources discussed in this section, both those newly detected in RRL emission and those previously known, have multiple observed velocity components. We can use GDIGS data with a method similar to the one described in Anderson et al. (2015b) to determine the “correct” velocity for some of these sources. For multiple RRL velocity H II regions in the GDIGS range we prepare Moment 0 maps of each measured velocity component by integrating over a velocity range equal to the full width at half maximum (FWHM) of the component and centered at the reported velocity. Each map is centered spatially on the WISE Catalog source. For

each region we visually compare the Moment 0 maps at the multiple velocities; the Moment 0 morphology at the “correct” velocity should match the angular size of the source in the WISE Catalog. The emission at the other velocity component(s) along the same line of sight is expected to be more spatially extended.

In Figure 1 we show an example of this method using the known H II region G010.331–00.287 from the WISE catalog. We display the GDIGS H α emission for the two detected velocities: 0.8 km s $^{-1}$ and 33.4 km s $^{-1}$ (Lockman 1989). The emission centered at the 0.8 km s $^{-1}$ velocity is diffuse and does not match the expected morphology. The emission centered at the 33.4 km s $^{-1}$ velocity matches the expected H II region morphology, and we therefore treat this as the “correct” H II region velocity.

As a point of comparison, in Figure 2 we show an example of an unsuccessful use of the method with H II region G019.494–00.150, also from the WISE Catalog. As in Figure 1 we display the GDIGS H α emission for the two detected velocities, this time at 32.1 km s $^{-1}$ and 54.6 km s $^{-1}$ (Anderson et al. 2011a). The emission observed from both velocity components has a good agreement with the size and location of the WISE Catalog entry; we therefore cannot determine which velocity is the “correct” one for the H II region.

Table 1. Multiple RRL Velocity Locations

Source	H II Region V_{LSR}	Other V_{LSR}
	(km s $^{-1}$)	(km s $^{-1}$)
G355.739+00.131	10.7	–77.4
G355.803–00.274	–31.5	3.1
G359.386–00.082	–134.2	–4.8
G359.648–00.083	–43.8	0.8
G359.717–00.036	–7.2	–60.0
G359.727–00.037	–7.2	–60.0
G000.729–00.103	83.2	105.3
G007.268–00.060	47.0	17.5
G007.380–00.264	31.8	9.7
G010.237–00.080	12.0	51.2
G010.331–00.278	33.4	0.8
G010.585–00.051	65.8	42.2
G011.840–00.191	49.7	9.0
G011.888–00.224	4.0	46.5
G012.311–00.059	67.3	30.5
G012.726–00.219	34.9	64.4
G015.010+00.049	26.5	63.5
G018.914–00.329	68.0	36.2
G019.466+00.168	19.9	70.8; 109.3
G019.494–00.150	32.1	54.6
G022.790–00.347	112.1	69.3
G022.987–00.155	100.2	76.6

Table 1 *continued*

Table 1 (*continued*)

Source	H II Region V_{LSR}	Other V_{LSR}
	(km s $^{-1}$)	(km s $^{-1}$)
G023.257–00.453	61.6	89.0
G024.826–00.265	44.7	109.8; 120.8
G024.919+00.294	108.6	135.1
G025.183+00.117	99.6	47.7; 56.7
G025.599–00.252	122.3	64.3; 114.2
G026.306+00.073	92.4	35.8
G028.605–00.013	41.9	92.8
G030.212–00.157	98.6	66.2
G030.248–00.102	102.9	67.9
G030.442–00.004	38.9	92.7; 109.2
G030.478–00.091	102.1	78.7; 47.2
G030.613–00.617	12.2	87.8; 110.2
G030.867+00.008	96.1	44.8

We compile a list of all 121 multiple-velocity H II regions in the GDIGS range from the WISE Catalog. We use GDIGS data to identify the LSR velocity of the discrete source for 35 of these 121 sources. We give the H II region velocity for these 35 sources in Table 1, which lists the source name, the H II region RRL velocity, and the other RRL velocities detected along the line of sight. The H II regions G359.717–00.036 and G359.727–00.037 are in close angular proximity and have the same reported velocities. In this case, the velocities reported in the WISE Catalog were obtained by previous observations that observed both objects in the same beam. Following the methodology of the WISE Catalog, we report the same velocity components for both. We were not able to distinguish the “correct” velocity for the remaining sources using our method. We hypothesize that the other velocities come from the DIG or from extended envelopes of other nearby H II regions.

We also use GDIGS data to verify a subset of the H II region velocities reported in Anderson et al. (2015a). In Anderson et al. (2015a) the authors attempted to determine the correct velocities of 117 multiple-velocity H II regions from the HRDS using new GBT RRL observations. We identified 60 H II regions in that paper that fall within the GDIGS survey area and applied the method described earlier in this section. None of these 60 sources showed a disagreement with the analysis of Anderson et al. (2015a). For 45 of these H II regions we successfully confirmed the previously reported velocities. We were unable to determine the velocities of the remaining 15, because we were not able to associate the morphology with that expected from the WISE Catalog.

3.1.2. Group H II Regions

GDIGS can provide RRL detections for “group” H II regions, which are found in complexes with other known

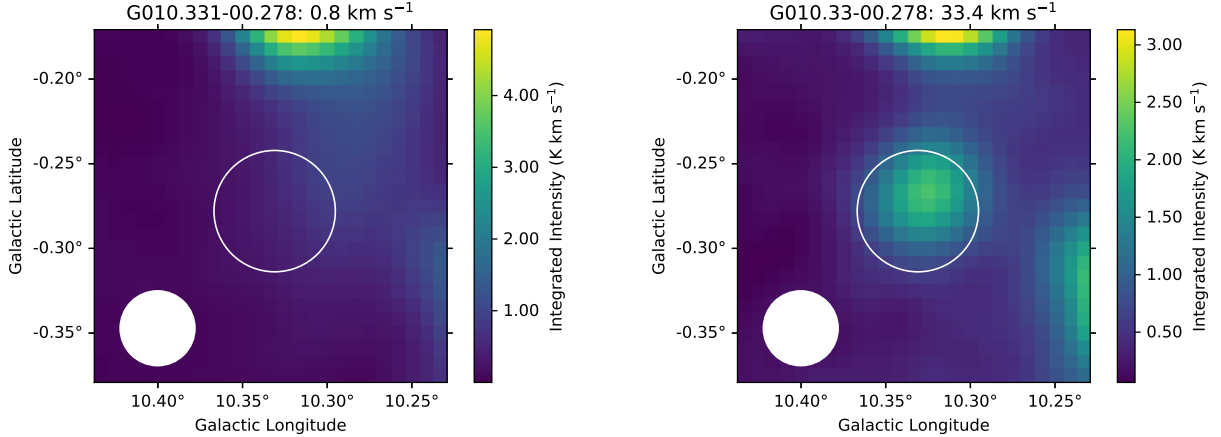


Figure 1. $\text{Hn}\alpha$ Moment 0 images toward source G010.331–0.278. Each image is integrated over a range centered at one of the two detected RRL velocities for this source and equal in width to the corresponding FWHM. The left image is integrated over a FWHM of 14.1 km s^{-1} with the range centered at 0.8 km s^{-1} , and the right image is integrated over a FWHM of 27.8 km s^{-1} with the range centered at 33.4 km s^{-1} (Lockman 1989). The solid white circles in the lower left corners show the $2''.65$ beam size. The 0.8 km s^{-1} emission is spatially extended, whereas the 33.4 km s^{-1} emission is spatially centered on G010.331–0.278 with an angular extent similar to that reported in the WISE Catalog (white circles). We conclude that the velocity of G010.331–0.278 is 33.4 km s^{-1} , and the 0.8 km s^{-1} component is from the DIG.

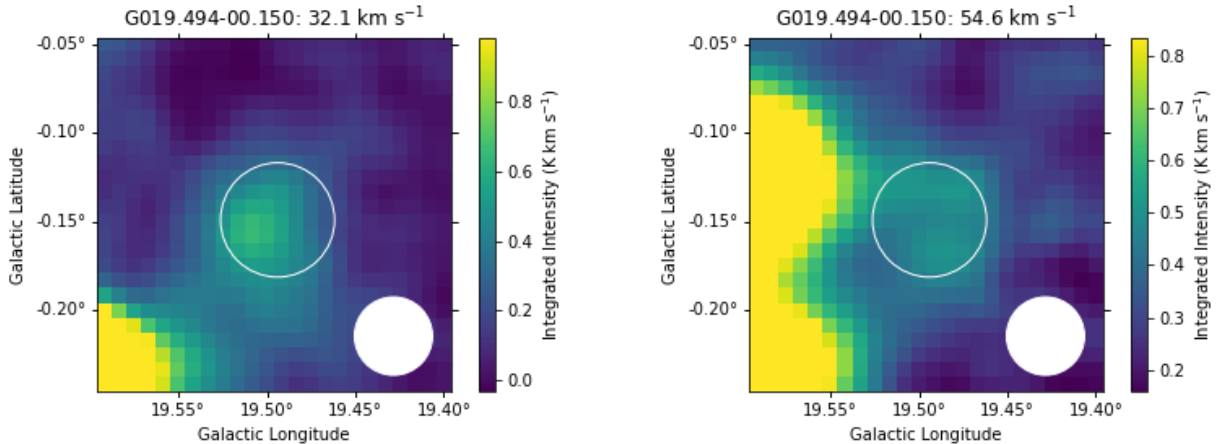


Figure 2. $\text{Hn}\alpha$ Moment 0 images toward source G019.494–0.150. Each image is integrated over a range centered at one of the two detected RRL velocities for this source and equal in width to the corresponding FWHM. The left image is integrated over a FWHM of 16.8 km s^{-1} with the range centered at 32.1 km s^{-1} , and the right image is integrated over a FWHM of 15.1 km s^{-1} with the range centered at 54.6 km s^{-1} (Anderson et al. 2011a). The solid white circles in the lower right corners show the $2''.65$ beam size. For both velocity components we see similar emission, and therefore are unable to discern which velocity component belongs to the H II region.

H II regions but have not been detected previously in pointed RRL surveys. There are ~ 160 WISE Catalog group H II regions in the GDIGS survey zone. Many of these are confused with brighter nearby H II regions, and so their RRL emission cannot be reliably measured. There are 40 unconfused group H II regions that we examine for RRL emission. We consider group H II regions unconfused if they are separated from their nearest neighbor by a beam width or more. For each of these, we extract a GDIGS $\text{Hn}\alpha$ spectrum by integrating over

a circle of radius given by the WISE Catalog. We then fit a Gaussian profile to each spectrum thus obtained.

We give the Gaussian fit parameters for the examined group H II regions in Table 2, which lists the source name, the Galactic longitude (ℓ) and latitude (b), the line intensity (T_L), the LSR velocity (V_{LSR}), the FWHM line width (ΔV), the rms noise, and the signal-to-noise ratio (S/N). The errors in Table 2 are 1σ uncertainties from the Gaussian fits. Of the 40 observed H II regions, 18 have multiple RRL velocity components. For those

sources, we apply the method described in Section 3.1.1. If the correct velocity can be determined, we report the correct velocity first, followed by the other velocity with an asterisk appended to the name. For sources for which we cannot determine which velocity is correct, we report both, appended with “a” and “b” in order of decreasing $\text{Hn}\alpha$ intensity. All listed line parameters have a S/N of at least three, where the S/N as defined by Lenz & Ayres (1992) is

$$S/N = 0.7 \left(\frac{T_L}{\text{rms}} \right) \left(\frac{\Delta V}{2.35} \right)^{0.5}, \quad (1)$$

where 2.35 is the FWHM in km s^{-1} of the spectral smoothing kernel we used when generating the spectra.

We expect to detect FWHM line widths between $\sim 10 \text{ km s}^{-1}$ and $\sim 35 \text{ km s}^{-1}$ (Anderson et al. 2011b). Line widths with values lower than 10 km s^{-1} imply electron temperatures $< 1100 \text{ K}$ (Anderson et al. 2018a). Line widths over $\sim 35 \text{ km s}^{-1}$ are very unlikely to be single components, so those reported here are likely the result of blended components.

3.1.3. *H II Region Candidates*

Within the GDIGS survey range there are ~ 400 WISE Catalog H II region candidates that have spatially coincident radio continuum and MIR emission but lack a spectroscopic ionized gas detection. Since the GDIGS area has been searched several times by sensitive, pointed RRL surveys (e.g., Anderson et al. 2011b, 2015c), new H II region detections using GDIGS are expected only for candidate sources that were skipped in previous surveys. We examine these ~ 400 locations and find 27 H II region candidates that are detected in the GDIGS $\text{Hn}\alpha$ data and are unconfused by the RRL emission from nearby bright H II regions, using the same criteria as in Section 3.1.2. We integrate GDIGS $\text{Hn}\alpha$ data over the extent of the sources defined in the WISE catalog and fit Gaussian components. We give the RRL parameters in Table 3. Eight of the nebulae are best fit with two Gaussian components. For these sources with multiple velocity components, we again apply the method described in Section 3.1.1. We use the same table format as that of Table 2 and the same S/N requirement as described in Section 3.1.2. Two candidates, G037.319+00.162 and G037.320+00.168, have low S/N values and appear to have blended peaks. Blended peaks occur where two emission peaks that are broad enough and close enough in velocity appear to merge together into one broad, flat-topped peak. We fit these candidates with two Gaussian components each.

3.1.4. *Radio-quiet H II Region Candidates*

Within the GDIGS survey range there are ~ 800 WISE Catalog radio quiet H II regions. These nebulae have the characteristic MIR morphology of H II regions, but have no detected radio continuum emission in any extant survey. Given the sensitivity of GDIGS, we therefore do not expect many $\text{Hn}\alpha$ RRL detections. In the Galactic longitude range $17.5^\circ > \ell > -5^\circ$, however, the quality of public radio continuum data suitable for identifying H II regions is poor so the pointed surveys may not have identified all detectable targets. In this range the GDIGS data may be able to provide RRL detections for some radio-quiet H II regions.

We measure RRL emission from 21 out of the 800 WISE Catalog radio quiet H II regions by integrating GDIGS $\text{Hn}\alpha$ data over the extent of the sources defined in the WISE catalog. All but one of these are in the zone $17.5^\circ > \ell > -5^\circ$. Four of these nebulae are best fit with two Gaussian components, and one with three Gaussian components. We give the $\text{Hn}\alpha$ RRL parameters in Table 4, with the same table format as that of Table 2 and the same S/N requirement as described in Section 3.1.2.

3.2. *New RRL Detections*

We discover 45 discrete sources in GDIGS that are not associated with objects in the WISE Catalog.

Some H II region candidates may have been missed by the WISE Catalog because their MIR emission is especially faint or because it was confused with other H II regions in close proximity. If the locations of discrete RRL emission coincide with MIR emission characteristic of H II regions, we categorize them as newly-discovered H II regions; if not, we characterize them as discrete emission zones. All WISE Catalog objects have coincident MIR emission, so the lack of coincident MIR is an important difference.

In addition, we identify several locations of RRL emission of particular interest because of their anomalously high LSR velocities. Because of these unusual velocities, we analyze this last category separately from the rest of the H II regions and discrete emission zones.

3.2.1. *Newly Discovered H II Regions*

There are eight compact locations of GDIGS RRL emission that are spatially coincident with MIR emission but are not in the WISE Catalog. We hypothesize that these are H II regions that were likely missed in the WISE Catalog because their MIR emission is faint or confused with that of other nearby regions. Of particular note is the relative faintness of these regions’ $8 \mu\text{m}$ emission compared to that of other H II regions. In all other respects these objects look like previously

Table 2. GDIGS H α RRL Parameters from WISE Catalog Group H II Regions

Source ^a	ℓ	b	T_L	σT_L	V_{LSR}	σV_{LSR}	ΔV	$\sigma \Delta V$	rms	S/N
	($^\circ$)	($^\circ$)	(mK)	(mK)	(km s $^{-1}$)	(km s $^{-1}$)	(km s $^{-1}$)	(km s $^{-1}$)	(mK)	
G004.613-00.150	4.614	-0.145	33.3	1.5	18.4	0.8	34.4	1.8	3.3	27.0
G008.153-00.198	8.098	-0.093	25.4	0.3	40.9	0.2	31.4	0.5	1.1	59.1
G008.181+00.321	8.183	0.320	33.5	1.0	22.9	0.4	23.9	0.8	2.0	37.4
G008.472-00.263	8.472	-0.262	36.3	1.4	36.0	0.6	32.8	1.5	3.4	27.9
G008.474-00.281	8.476	-0.280	69.0	1.7	38.6	0.3	24.8	0.7	3.2	49.0
G009.381-00.067	9.385	-0.076	9.1	0.9	49.1	2.6	55.2	6.1	2.6	11.9
G009.599+00.165	9.597	0.168	40.2	2.0	4.6	0.5	20.7	1.2	3.6	23.2
G010.227-00.346	10.233	-0.349	99.5	1.0	15.4	0.2	36.8	0.4	2.4	114.8
G010.321-00.266	10.322	-0.265	85.2	1.5	32.0	0.3	30.0	0.6	2.9	73.4
G010.321-00.266*	10.322	-0.265	43.0	0.6	1.5	1.2	19.4	0.4	2.9	29.8
G010.441+00.012a	10.441	0.011	104.1	1.6	71.9	0.2	22.6	0.4	2.7	83.7
G010.441+00.012b	10.441	0.011	18.2	1.8	42.9	6.1	54.8	9.0	2.7	22.8
G010.453-00.006a	10.455	-0.005	62.6	1.5	69.1	0.3	23.8	0.7	2.4	58.1
G010.453-00.006b	10.455	-0.005	29.7	0.6	42.3	0.7	30.1	1.5	2.4	31.0
G010.497+00.028a	10.498	0.029	42.9	0.8	66.6	0.2	24.0	0.6	2.9	33.1
G010.497+00.028b	10.498	0.029	27.0	0.4	44.5	0.3	21.0	0.8	2.9	19.5
G010.617-00.405	10.619	-0.400	287.8	2.0	-1.4	0.1	24.6	0.2	5.1	127.8
G010.966+00.022	10.968	0.024	66.2	1.8	17.4	0.4	29.1	0.9	4.0	39.8
G012.683-00.185a	12.682	-0.184	226.7	2.2	52.8	0.1	24.5	0.4	4.7	109.0
G012.683-00.185b	12.682	-0.184	133.3	2.5	34.3	0.3	18.7	0.8	4.7	56.0
G012.692-00.251	12.688	-0.245	197.7	1.9	33.5	0.1	16.1	0.2	3.3	109.4
G012.692-00.251*	12.688	-0.245	105.2	1.6	55.1	0.2	21.0	0.5	3.3	66.7
G012.820-00.238a	12.873	-0.234	161.9	1.5	32.6	0.1	25.5	0.3	2.7	138.3
G012.820-00.238b	12.873	-0.234	25.4	1.8	63.1	1.9	18.7	3.4	2.7	18.6
G012.884-00.237	12.818	-0.243	326.0	2.0	32.9	0.1	27.6	0.2	3.8	205.8
G012.884-00.237*	12.818	-0.243	55.0	2.2	59.2	1.2	22.7	2.3	3.9	31.5
G012.891-00.195a	12.894	-0.195	58.7	0.6	33.7	0.1	25.0	0.3	3.5	38.3
G012.891-00.195b	12.894	-0.195	21.0	0.9	62.6	0.5	22.3	1.4	3.5	12.9
G016.258-00.091	16.254	-0.090	34.9	0.9	42.8	0.4	34.6	1.0	2.0	46.9
G016.352-00.179	16.349	-0.176	96.5	1.5	45.4	0.2	26.6	0.5	3.4	66.8
G017.073-00.096	17.082	-0.092	47.8	0.5	93.7	0.1	24.6	0.3	2.6	41.6
G017.073-00.096*	17.082	-0.092	10.0	0.3	36.7	0.9	41.5	2.5	2.6	11.3
G018.441+00.013	18.441	0.014	46.5	1.8	61.9	0.6	33.2	1.5	3.8	32.2
G024.093+00.455	24.094	0.456	15.0	0.2	85.9	0.3	44.1	0.8	1.7	26.8
G024.525-00.041	24.528	-0.046	60.2	0.4	97.8	0.2	54.0	0.5	1.8	112.2
G024.640-00.142a	24.648	-0.139	100.2	0.5	103.3	0.1	41.9	0.3	2.6	53.5
G024.640-00.142b	24.648	-0.139	47.5	0.5	38.8	0.2	41.2	0.6	2.6	113.9
G025.179+00.038	25.177	0.028	17.3	0.3	44.4	0.4	48.2	1.1	1.6	34.3
G025.179+00.038*	25.177	0.028	12.0	0.2	91.3	0.7	56.0	1.9	1.6	25.6
G028.185+00.314	28.186	0.316	7.3	0.8	45.8	2.4	40.0	6.2	1.9	11.1
G028.185+00.314*	28.186	0.316	8.7	0.8	95.1	2.3	46.0	6.1	1.9	14.2
G028.670+00.011	28.670	0.008	122.0	0.9	102.5	0.1	28.6	0.2	4.1	72.7
G028.670+00.011*	28.670	0.008	15.8	0.6	41.1	0.3	19.1	0.9	4.1	7.7
G028.702+00.014a	28.704	0.014	91.6	0.9	103.7	0.2	33.3	0.4	3.7	65.2
G028.702+00.014b	28.704	0.014	15.2	0.5	39.3	0.4	23.7	1.0	3.7	9.1
G029.814-00.069	29.862	-0.083	204.6	1.0	97.8	0.1	24.1	0.1	1.6	286.7
G029.862-00.059	29.862	-0.059	286.2	1.9	96.4	0.1	21.5	0.2	3.3	183.6
G029.889-00.007	29.887	-0.002	220.5	1.0	96.7	0.1	26.6	0.1	1.6	324.6
G029.901-00.029	29.904	-0.025	147.7	0.7	96.4	0.1	26.4	0.1	1.2	288.8
G029.928-00.057	29.927	-0.058	464.2	1.7	98.5	0.1	29.4	0.1	2.8	410.5
G029.955-00.093	29.963	-0.091	173.1	1.1	96.5	0.1	28.6	0.2	2.1	201.3
G030.007-00.084	30.010	-0.085	155.8	1.2	95.6	0.1	23.9	0.2	2.5	139.1
G031.264+00.031a	31.265	0.033	62.9	0.6	101.7	0.1	26.0	0.3	2.6	56.3
G031.264+00.031b	31.265	0.033	18.6	0.3	35.9	0.4	45.7	1.1	2.6	22.1
G031.309+00.044	31.310	0.039	63.3	1.7	101.8	0.1	23.7	0.3	2.1	67.1
G031.309+00.044*	31.310	0.039	12.8	0.2	38.3	0.4	41.7	1.2	2.1	18.0
G031.422-00.256	31.432	-0.249	106.4	1.1	88.5	0.2	32.1	0.4	1.8	152.9
G031.422-00.256*	31.432	-0.249	14.8	0.2	41.5	0.5	37.5	1.2	1.8	23.0

^a Source names for HII regions with multiple detected hydrogen RRL components are appended with “a” and “b” in order of decreasing H α RRL intensity. Source names for additional velocity components for sources with successfully determined “correct” velocities are appended with an asterisk.

Table 3. GDIGS Hn α RRL Parameters from WISE Catalog Candidate H II Regions

Source ^a	ℓ	b	T_L	σT_L	V_{LSR}	σV_{LSR}	ΔV	$\sigma \Delta V$	rms	S/N
	($^\circ$)	($^\circ$)	(mK)	(mK)	(km s ⁻¹)	(km s ⁻¹)	(km s ⁻¹)	(km s ⁻¹)	(mK)	
G355.681+00.143	355.681	0.147	40.8	0.5	-76.5	0.1	14.3	0.2	1.8	39.1
G355.681+00.143*	355.681	0.147	24.5	0.4	7.0	0.2	18.1	0.4	1.8	26.4
G355.727-00.212	355.727	0.212	58.3	0.9	-76.9	0.1	11.1	0.2	2.1	42.2
G355.727-00.212*	355.727	0.212	20.7	0.3	7.7	0.2	22.2	0.4	2.1	21.2
G359.690+00.065	359.690	0.065	22.4	0.7	-90.0	0.7	41.1	1.6	3.0	24.9
G359.690+00.065*	359.690	0.065	27.9	0.7	5.4	0.3	22.5	0.7	3.0	22.1
G000.132+00.039	0.132	0.040	341.2	1.3	-17.3	0.1	57.2	0.3	12.4	95.0
G000.551+00.060	0.551	0.060	60.4	0.6	52.0	0.3	50.2	0.7	3.1	63.0
G000.551+00.060*	0.551	0.060	22.2	0.5	8.7	1.3	47.0	3.2	3.1	22.4
G000.591+00.050	0.592	0.050	58.1	0.8	56.0	0.3	37.7	0.7	3.6	45.2
G000.591+00.050*	0.592	0.050	21.3	0.5	6.2	0.6	42.2	1.5	3.6	17.6
G016.770+00.019	16.770	0.020	18.8	0.9	32.8	0.8	32.3	1.9	5.5	8.9
G020.427-00.074	20.427	-0.074	24.6	0.6	49.2	0.4	28.2	0.8	3.8	15.7
G021.404-00.238	21.404	-0.237	16.5	0.8	80.1	0.7	30.5	1.6	4.4	9.5
G021.474-00.156	21.475	-0.156	8.6	0.4	77.8	1.0	49.3	2.5	2.6	10.6
G021.494-00.159	21.494	-0.158	8.6	0.3	80.4	1.0	53.2	2.4	2.6	11.0
G021.521-00.253	21.521	-0.253	11.5	0.2	72.8	0.6	62.6	1.5	2.1	19.8
G021.827+00.042a	21.827	0.043	21.2	0.4	22.4	0.3	39.2	0.9	2.0	30.3
G021.827+00.042b	21.827	0.043	8.6	0.2	90.4	0.7	44.0	2.0	2.0	13.0
G024.082+00.121	24.082	0.121	18.9	0.1	88.6	0.3	70.2	0.7	1.3	55.6
G024.114-00.183	24.114	-0.183	21.2	0.1	80.2	0.2	49.7	0.5	1.1	62.0
G025.330-00.461	25.330	-0.460	15.9	0.3	61.0	0.4	53.9	1.1	1.1	48.5
G026.613+00.309	26.614	0.309	17.0	0.4	106.5	0.4	28.2	0.9	1.7	24.2
G026.718-00.385	26.719	-0.384	18.5	0.4	86.1	0.4	37.1	1.0	1.5	34.3
G027.720-00.106	27.720	-0.105	18.1	0.5	91.6	0.3	27.7	0.8	2.3	18.9
G028.024-00.162	28.024	-0.162	26.5	0.3	103.3	0.2	33.0	0.4	1.9	36.6
G028.078+00.144	28.079	0.144	17.8	0.4	87.9	0.5	44.5	1.3	2.8	19.4
G028.438+00.033	28.438	0.033	28.2	0.7	94.5	0.4	33.5	0.9	4.6	16.2
G029.007-00.289	29.009	-0.288	13.9	0.2	92.9	0.3	39.8	0.6	1.0	40.0
G031.243+00.274	31.243	0.274	24.3	0.6	98.9	0.3	26.1	0.7	3.0	18.9
G031.243+00.274*	31.243	0.274	9.2	0.5	38.9	0.9	30.9	2.1	3.0	7.8
G032.034-00.375	32.034	-0.375	23.6	0.4	44.4	0.2	21.1	0.5	1.8	27.5
G032.034-00.375*	32.034	-0.375	6.3	0.3	85.4	1.0	35.6	2.6	1.8	9.5
G037.319+00.162a	37.319	0.162	7.4	1.3	26.6	3.2	36.6	8.4	2.7	11.4
G037.319+00.162b	37.319	0.162	6.7	1.0	62.7	6.2	56.9	15.6	2.7	8.5
G037.320+00.168a	37.321	0.169	7.4	1.1	67.6	5.2	56.0	13.6	2.9	10.3
G037.320+00.168b	37.321	0.169	6.7	1.3	28.6	5.7	47.0	14.6	2.9	7.2

^aSource names for HII regions with multiple detected hydrogen RRL components are appended with “a” and “b” in order of decreasing Hn α RRL intensity. Source names for additional velocity components for sources with successfully determined “correct” velocities are appended with an asterisk.

Table 4. GDIGS H α RRL Parameters from WISE Catalog Radio-quiet H II Regions

Source ^a	ℓ	b	T_L	σT_L	V_{LSR}	σV_{LSR}	ΔV	$\sigma \Delta V$	rms	S/N
	($^\circ$)	($^\circ$)	(mK)	(mK)	(km s ⁻¹)	(km s ⁻¹)	(km s ⁻¹)	(km s ⁻¹)	(mK)	
G359.901-00.320	359.901	-0.319	100.1	1.0	15.0	0.1	24.2	0.3	2.3	97.8
G000.408-00.881	0.408	-0.881	54.7	0.5	14.0	0.1	18.9	0.2	2.5	43.4
G000.456-00.808	0.456	-0.808	46.6	0.4	14.0	0.1	20.1	0.2	2.1	45.4
G000.477-00.130	0.477	-0.130	56.7	0.5	29.8	0.3	54.7	0.7	2.3	83.3
G000.834-00.457	0.835	-0.457	22.4	0.3	17.7	0.1	22.7	0.3	0.9	54.1
G001.119-00.266	1.119	-0.266	42.4	0.6	2.4	0.2	24.7	0.4	1.7	56.6
G003.627+00.087	3.628	0.087	18.8	0.5	9.4	0.4	36.4	1.1	3.1	16.7
G004.270+00.038	4.270	0.039	18.9	0.7	9.8	0.5	28.2	1.2	3.6	12.7
G006.256-00.074	6.257	-0.073	52.3	0.6	20.8	0.2	33.2	0.4	2.7	51.0
G008.359+00.003	8.360	0.004	29.7	0.4	26.0	0.3	48.3	0.8	1.9	49.6
G008.685-00.047	8.685	-0.046	15.4	0.2	30.1	0.4	51.6	1.1	1.4	36.1
G009.070+00.082	9.071	0.082	9.9	0.3	31.2	0.8	57.1	2.2	1.9	18.0
G010.518-00.289	10.518	-0.288	26.9	0.7	0.0	0.2	19.0	0.6	1.5	35.7
G010.518-00.289*	10.518	-0.288	4.4	0.2	38.2	1.8	56.7	4.3	1.5	10.1
G011.822-00.097	11.822	-0.097	49.7	1.2	61.3	0.3	22.5	0.6	1.8	59.8
G011.822-00.097*	11.822	-0.097	12.9	0.4	9.7	0.4	25.9	1.0	1.8	16.7
G011.822-00.097*	11.822	-0.097	6.5	0.2	118.5	0.9	34.5	2.7	1.8	9.7
G011.887-00.253a	11.888	-0.253	37.9	0.4	48.9	0.1	22.3	0.3	1.7	48.1
G011.887-00.253b	11.888	-0.253	12.8	0.3	7.7	0.4	29.8	1.0	1.7	18.8
G012.051-00.171	12.051	-0.171	37.1	0.7	39.8	0.2	22.6	0.5	4.2	19.2
G012.161-00.186	12.161	-0.186	35.2	0.3	38.3	0.2	40.0	0.5	1.8	56.5
G012.515+00.066	12.516	0.067	15.4	0.3	54.0	0.3	22.5	0.8	1.3	25.7
G012.515+00.066*	12.516	0.067	34.4	0.4	28.8	0.1	24.4	0.4	1.3	59.7
G014.068-00.432a	14.068	-0.432	31.1	0.4	26.0	0.2	32.8	0.6	1.8	45.2
G014.068-00.432b	14.068	-0.432	18.1	0.2	47.9	0.6	40.5	1.3	1.8	29.2
G017.037+00.320	17.038	0.321	20.5	0.3	19.7	0.2	32.3	0.5	1.7	31.3
G037.642+01.192	37.643	1.193	7.9	0.2	42.9	0.4	29.3	0.9	1.1	17.8

^aSource names for H II regions with multiple detected hydrogen RRL components are appended with “a” and “b” in order of decreasing H α RRL intensity. Source names for additional velocity components for sources with successfully determined “correct” velocities are appended with an asterisk.

known H II regions, and we do not have enough information to determine whether the deficiency in $8\mu\text{m}$ emission reflects an inherent difference significant enough to put these objects into a different class. We measure RRL emission from these new H II regions by integrating GDIGS H α data over their extents defined visually from $24\mu\text{m}$ MIR data. The RRL emission from three of these nebulae is best fit with two Gaussian components, and one with three Gaussian components. We characterize the H α GDIGS emission from these locations in Table 5. The table format is the same as that of Table 2, with the addition of the region radius. We use the same method for determining the correct velocity as described in Section 3.1.1 and the same S/N requirement as described in Section 3.1.2.

3.2.2. Discrete Emission Zones (DEZs)

We discover 30 locations of GDIGS H α emission in the Moment 0 maps that lack the spatially coincident MIR emission expected of H II regions and also lack the expected radio continuum emission of supernova rem-

nants (SNRs). We call these 30 locations discrete emission zones (DEZs). MIR emission is present for all known Galactic H II regions, including those discovered in older surveys that targeted radio continuum emission peaks (e.g. Lockman 1989). We likewise expect MIR emission from planetary nebulae (Anderson et al. 2012). Most SNRs lack MIR emission (Fuerst et al. 1987), and because they are non-thermal radio sources, are not expected to be strong in RRL emission (Liu et al. 2019). Any RRL emission from SNRs is expected to occur at frequencies lower than those observed in GDIGS.

With available data, we cannot conclusively categorize the emission sources, and here we only characterize their H α emission properties. We measure RRL emission from these locations by integrating GDIGS H α data over their extents defined by visually fitting circles using the GDIGS Moment 0 map. Of the 30 nebulae, 11 are best fit with two Gaussian components, and one with three Gaussian components. We give the GDIGS H α line parameters locations in Table 6. The table format is the same as that of Table 5. We use the same method

Table 5. GDIGS H α RRL Parameters from New H II Regions

Source ^a	ℓ	b	Radius	T_L	σT_L	V_{LSR}	σV_{LSR}	ΔV	$\sigma \Delta V$	rms	S/N
	($^\circ$)	($^\circ$)	($''$)	(mK)	(mK)	(km s^{-1})	(km s^{-1})	(km s^{-1})	(km s^{-1})	(mK)	
G357.626-00.082	357.626	-0.082	190	4.4	0.3	3.1	1.2	37.5	2.9	2.3	5.3
G012.522-00.121	12.522	-0.121	273	32.9	0.5	47.1	0.3	21.8	0.6	1.8	39.0
G012.522-00.121*	12.522	-0.121	273	72.5	1.2	29.3	0.1	16.7	0.4	1.8	75.2
G012.576+00.221	12.576	0.221	217	30.2	0.4	20.8	0.2	23.6	0.4	1.8	37.3
G020.805+00.019	20.805	0.019	581	49.8	0.5	52.3	0.1	29.5	0.3	1.3	95.0
G028.567+00.002	28.567	0.002	191	68.4	0.5	97.5	0.1	33.5	0.3	2.7	67.0
G028.567+00.002*	28.567	0.002	191	18.5	0.4	41.3	0.3	27.2	0.7	2.7	16.2
G028.618+00.177a	28.618	0.178	655	21.4	0.4	103.0	0.3	31.1	0.6	1.0	54.5
G028.618+00.177b	28.618	0.178	655	5.7	0.2	33.4	0.5	26.1	1.5	1.0	13.3
G028.618+00.177c	28.618	0.178	655	5.3	0.2	68.2	0.9	33.4	3.4	1.0	14.0
G030.820-00.764	30.820	-0.764	666	18.0	0.2	81.4	0.2	36.1	0.6	0.9	54.9
G042.634+00.125	42.634	0.125	132	13.0	0.3	12.9	0.4	32.6	1.2	1.9	28.2
G042.634+00.125*	42.634	0.125	132	8.7	0.3	63.1	0.6	36.4	1.5	1.9	20.0

^a Source names for HII regions with multiple detected hydrogen RRL components are appended with “a” and “b” in order of decreasing H α RRL intensity. Source names for additional velocity components for sources with successfully determined “correct” velocities are appended with an asterisk.

for determining the correct velocity as described in Section 3.1.1 and the same S/N requirement as described in Section 3.1.2. For these DEZs, the “correct” velocity is the one that best matches the emission seen in the initial Moment 0 maps integrated over all velocities.

3.2.3. Anomalous Velocity Features

We identify 10 emission zones in the GDIGS H α Moment 0 maps that are not known to be H II regions and have anomalously high velocities compared to that of other H II regions at the same Galactic longitudes. We call such emission zones anomalous velocity features (AVFs) and estimate their positions and radii by visually fitting circles to the emission in the GDIGS H α Moment 0 map.

For each of the 10 AVFs, we extract a GDIGS H α spectrum by integrating over the extent of the source. To each such spectrum we then fit a Gaussian profile.

We designate the 10 identified AVFs by their Galactic latitude and longitude. We provide the Gaussian fit parameters in Table 7. The table format is the same as that of Table 5. We use the same method for determining the correct velocity as described in Section 3.1.1 and the same S/N requirement as described in Section 3.1.2.

4. DISCUSSION

4.1. WISE Catalog H II regions

Because H II regions are formed by short-lived massive stars, a sufficiently large sample of H II regions with known distances can be used to measure the current properties of Galactic massive star formation (Anderson et al. 2018a). The present work adds H II regions avail-

able to such studies by confirming 27 H II region candidates, 21 radio-quiet H II regions, and 40 group H II regions as known H II regions, adding eight previously unreported H II regions, and confirming the velocities of 35 previously known H II regions. These numbers are tabulated in Table 8. Together, these 131 new velocity measurements represent a 5.6% increase in the number of WISE Catalog objects with a known velocity.

The GDIGS RRL velocities of group H II regions indicate that they are for the most part correctly associated with known H II regions. Of the 40 observed group H II regions, 38 have one observed LSR velocity within 10 km s^{-1} of the “group velocity” (the velocity measured for the H II region complex) reported in the WISE Catalog; all have one component within 20 km s^{-1} . In Figure 3, we plot the differences between the measured GDIGS group H II region RRL velocity and the group velocity as reported in the WISE Catalog. H II regions with multiple observed velocities are excluded from this plot. There is a strong correlation between the two velocities, indicating that the original group associations for this sample were largely correct.

4.2. DEZs

Ionized gas comprises a significant portion of the Galactic ISM, accounting for more than 20% of the Milky Way’s gas mass (Reynolds 1991). Despite this, current understanding of the ionized component of the ISM is far from complete. The identification and characterization here of 30 discrete zones of RRL emission suggests that the Galactic DIG may consist in part of compact emission zones with sizes of a few arcminutes.

Table 6. GDIGS H α RRL Parameters from Discrete Emission Zones

Source ^a	ℓ	b	Radius	T_L	σT_L	V_{LSR}	σV_{LSR}	ΔV	$\sigma \Delta V$	rms	S/N
	($^\circ$)	($^\circ$)	($''$)	(mK)	(mK)	(km s^{-1})	(km s^{-1})	(km s^{-1})	(km s^{-1})	(mK)	
G357.627-00.415	357.627	-0.415	466	16.9	0.4	9.1	0.3	26.3	0.7	2.1	18.8
G358.414-00.122a	358.414	-0.122	229	4.1	0.4	12.3	1.3	29.1	3.2	2.4	4.2
G358.414-00.122b	358.414	-0.122	229	2.6	0.4	-213.7	3.5	50.2	8.6	2.4	3.5
G358.460-00.170	358.460	-0.170	229	4.2	0.4	10.6	1.0	24.1	2.5	2.1	4.5
G358.918-00.195	358.918	-0.195	190	11.1	0.2	3.9	0.4	38.4	0.9	1.5	20.9
G003.415+00.171	3.415	0.171	229	12.7	0.3	10.3	0.5	46.6	1.3	1.7	23.3
G004.537-00.288	4.537	-0.288	592	16.2	0.1	12.5	0.1	34.1	0.3	1.2	36.0
G007.044+00.018	7.044	0.018	752	30.1	0.3	22.8	0.2	35.0	0.4	1.2	67.8
G009.875-00.160	9.875	-0.160	399	18.2	0.4	29.7	0.3	25.5	0.6	2.1	20.0
G012.289-00.327	12.289	-0.327	132	30.9	0.6	42.9	0.4	35.5	0.8	3.6	23.4
G012.508-00.127	12.508	-0.127	217	43.0	0.6	48.8	0.2	19.0	0.4	1.8	47.5
G012.508-00.127*	12.508	-0.127	217	64.7	1.4	28.7	0.2	16.7	0.5	1.8	67.1
G012.548-00.293	12.548	-0.293	132	68.1	1.3	29.7	0.1	16.2	0.3	2.4	52.2
G012.584-00.119	12.584	-0.119	289	91.3	1.1	31.1	0.1	17.3	0.2	2.0	86.7
G012.586-00.238	12.586	-0.238	132	88.4	1.3	31.0	0.1	15.0	0.3	2.3	68.0
G012.641-00.292	12.641	-0.292	404	88.7	0.7	33.2	0.1	15.0	0.2	2.9	54.1
G012.641-00.292*	12.641	-0.292	404	28.8	0.6	57.8	0.3	22.4	0.7	2.9	21.5
G012.643-00.357	12.634	-0.357	132	82.0	1.2	31.9	0.1	13.6	0.2	4.6	30.0
G013.642+00.236	13.642	0.236	132	22.4	0.4	35.9	0.4	48.0	0.9	2.6	27.3
G013.671-00.381a	13.671	-0.381	132	11.9	0.6	33.5	4.2	81.1	12.8	1.8	27.4
G013.671-00.381b	13.671	-0.381	132	5.5	0.7	121.7	4.4	59.7	11.5	1.8	10.9
G013.747-00.407	13.747	-0.407	132	17.0	0.7	37.2	0.6	31.4	1.4	3.9	11.2
G013.817-00.105a	13.817	-0.105	132	51.0	0.7	41.1	0.2	26.4	0.5	2.3	52.0
G013.817-00.105b	13.817	-0.105	132	17.6	0.5	106.0	0.3	19.1	0.7	2.3	15.3
G013.820-00.250	13.820	-0.250	132	15.2	0.4	102.9	0.3	21.6	0.8	2.1	15.4
G013.820-00.250*	13.820	-0.250	132	14.0	0.4	39.5	0.7	49.9	1.9	2.1	21.5
G015.238-00.364	15.238	-0.364	132	29.4	0.6	20.4	0.4	34.8	0.9	4.7	16.9
G015.238-00.364*	15.238	-0.364	132	16.4	1.2	58.3	0.3	9.2	0.8	4.7	4.8
G016.816+00.353	16.816	0.353	132	30.7	0.9	27.6	0.4	28.6	0.9	5.2	14.4
G017.187-00.207a	17.187	-0.207	110	20.4	0.4	43.9	0.3	26.5	0.8	3.1	15.5
G017.187-00.207b	17.187	-0.207	110	12.6	0.5	97.2	0.6	28.2	1.4	3.1	9.9
G017.187-00.207c	17.187	-0.207	110	7.2	0.4	-4.5	1.1	34.0	2.8	3.1	6.2
G017.768-00.075	17.768	-0.075	132	15.0	0.3	52.0	0.3	34.3	0.8	2.1	19.1
G025.511+00.068	25.511	0.068	186	21.3	0.5	57.2	0.5	30.0	1.3	2.2	24.2
G025.511+00.068*	25.511	0.068	186	13.5	0.3	105.1	0.7	48.1	2.0	2.2	19.4
G026.584+00.163	26.584	0.163	289	36.3	0.4	105.6	0.1	24.0	0.3	1.5	54.1
G026.584+00.163*	26.584	0.163	289	7.8	0.3	32.2	0.5	27.2	1.4	1.5	12.4
G027.128+00.010	27.128	0.010	425	39.3	0.4	92.5	0.2	28.1	0.4	2.3	41.4
G029.388+00.156a	29.388	0.156	189	16.5	0.2	48.9	0.3	42.9	0.8	1.9	26.0
G029.388+00.156b	29.388	0.156	189	12.9	0.2	98.3	0.4	44.5	1.1	1.9	20.7
G042.735-00.112	42.735	-0.112	442	18.9	0.2	68.2	0.1	21.1	0.3	1.3	30.5
G042.735-00.112*	42.735	-0.112	442	4.5	0.2	21.2	0.5	24.8	1.2	1.3	7.9
G043.379-00.064	43.379	-0.064	132	6.8	0.2	60.1	1.1	59.3	2.5	2.0	12.0

^a Source names for HII regions with multiple detected hydrogen RRL components are appended with “a” and “b” in order of decreasing H α RRL intensity. Source names for additional velocity components for sources with successfully determined “correct” velocities are appended with an asterisk.

The H α RRL morphology of the DEZs is generally centrally-peaked. Some DEZs have nearly circular RRL emission, some are oblong, and some are irregular in shape. In Figure 4 we show an example Moment 0 map of a typical DEZ, G018.641-00.296.

We examine 21 cm radio continuum emission from the Very Large Array (VLA) Galactic Plane Survey (VGPS) at the locations of the 11 DEZs that fall

within the VGPS survey area and found identifiable radio continuum emission for G026.584+00.163 and G027.128+00.010.

One of the DEZs, G012.508-00.127, has very faint 24 μm emission near its center, but lacks the 8 μm emission we also require from HII regions.

4.3. AVFs

Table 7. Anomalous Velocity Features (AVFs)

Source	ℓ	b	Radius	T_L	σT_L	V_{LSR}	σV_{LSR}	ΔV	$\sigma \Delta V$	rms	S/N
	($^\circ$)	($^\circ$)	($''$)	(mK)	(mK)	(km s^{-1})	(km s^{-1})	(km s^{-1})	(km s^{-1})	(km s^{-1})	
G355.612+00.314	355.612	0.314	390	9.1	1.2	101.2	1.7	24.7	3.9	1.5	13.8
G001.702-00.156	1.702	-0.156	234	8.1	1.2	227.3	1.3	17.9	3.0	1.7	9.2
G003.158-00.040	3.518	-0.040	105	5.7	1.1	150.7	3.0	32.0	7.0	2.4	6.1
G006.085-00.016	6.085	-0.016	225	5.0	1.1	139.9	3.2	28.6	7.4	1.6	7.6
G009.402+00.180	9.402	0.180	415	9.2	1.7	131.5	0.5	5.1	1.1	1.4	6.8
G011.936+00.020	11.936	0.020	285	6.4	1.8	120.5	2.7	19.2	6.3	1.7	7.5
G012.380-00.081	12.380	-0.081	445	5.5	1.3	118.5	2.5	18.8	5.3	1.3	8.4
G013.782-00.152	13.782	-0.152	501	11.0	0.6	102.8	0.7	26.2	1.7	1.2	21.4
G014.549-00.106	14.549	-0.106	398	10.5	1.6	150.5	1.9	26.0	4.6	1.2	20.4
G020.206+00.036	20.206	0.036	251	12.6	1.3	117.2	0.8	16.3	1.9	1.9	12.2

Table 8. New RRL Detections by Category

Source Category	Number
WISE Catalog Objects	
H II Region Candidates	27
Radio-Quiet H II Region Candidates	21
Group H II Regions	40
Known H II Regions	35
New H II Regions	8
DEZs	30
AVFs	10

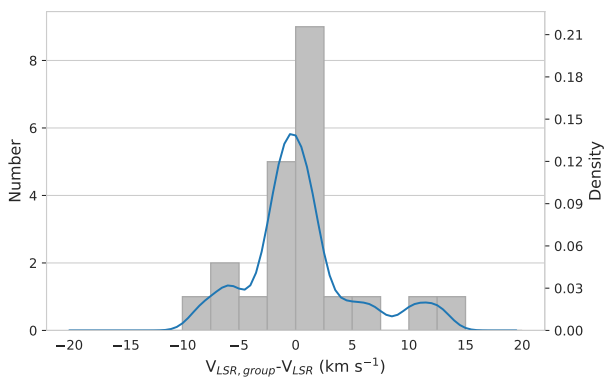


Figure 3. Histogram of differences between the measured GDIGS RRL velocity of 22 group H II regions and the group velocity reported in the WISE Catalog, overlaid with the kernel density estimate (KDE) curve for the same. The 18 H II regions with multiple velocity components have been excluded. The group H II regions all have velocities within 20 km s^{-1} of the velocities of their H II region complexes.

The ten objects that we call AVFs merit further study. They do not fit neatly into current models of gas behavior in the Galactic disk (Reid et al. 2019), and their existence may require an update to those models. We plan additional observations in order to better under-

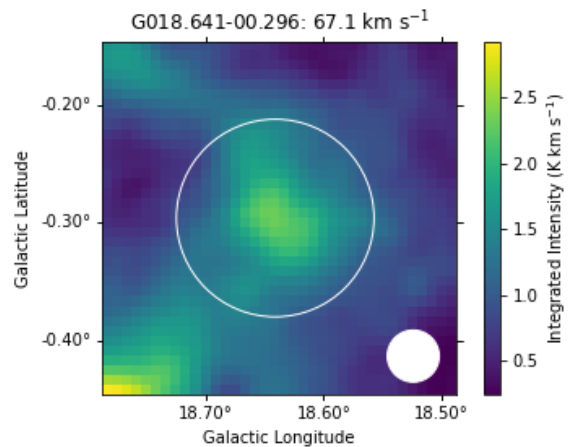


Figure 4. Example $\text{Hn}\alpha$ Moment 0 map of the DEZ G018.641-00.296. The image is integrated over a range centered at the velocity detected for this DEZ, 67.1 km s^{-1} and equal in width to the detected FWHM, 36.8 km s^{-1} . The white circle marks the estimated extent of the DEZ. The filled white circle in the lower right corner shows the 2.65 GDIGS beam size.

stand the origins of these objects and the reason for their high velocities.

To investigate the nature of these features, we compare GDIGS RRL data with the MIR data described in Section 2.2, as well as with HI from the Galactic All-Sky Survey (GASS; McClure-Griffiths et al. 2009), and with $^{13}\text{CO } J = 2 \rightarrow 1$ spectra from the Structure, Excitation, and Dynamics of the Inner Galactic ISM survey (SEDIGISM; Schuller et al. 2020) and the $J = 1 \rightarrow 0$ from the Galactic Ring Survey (GRS; Jackson et al. 2006). GASS has a spectral resolution of 0.82 km s^{-1} and a sensitivity of 57 mK . SEDIGISM has $1.0 \text{ K } 1\sigma$ sensitivity, $30''$ angular resolution, and 0.35 km s^{-1} spectral resolution. The GRS has $46''$ angular resolution, 0.2 km s^{-1} spectral resolution, and 0.4 K

sensitivity. We compare our RRL observations to ^{13}CO data from these surveys to search for any associated molecular gas, which is commonly found for Galactic H II regions. (Anderson & Bania 2009).

We show sample spectra, Moment 0 maps, and MIR maps in Figure 5. The complete figure set (30 images) can be found in the online version of this article. Morphologically, the RRL Moment 0 maps of AVFs have areas of bright emission with adjacent diffuse emission. In half of the AVFs the bright emission is concentrated in one clump, while in the other half it is split between two to three smaller clumps connected by diffuse emission. Two of the latter group have a structure resembling a shell. In eight out of ten cases each bright area has diffuse emission in all directions that gradually decreases in intensity. In the remaining two AVFs the intensity of GDIGS emission drops off sharply in at least one direction. The individual clumps vary in shape between compact, oblong, and irregular structures. The wide variety of morphologies seen in the AVFs further confounds attempts to determine their nature and origin, and raises the possibility that the AVFs might not all be the same type of object.

We compare AVF observations with MIR data to determine if the objects may be H II regions, and find that none have the associated $24\ \mu\text{m}$ emission that is characteristic of H II regions. Nine have $24\ \mu\text{m}$ MIR emission near to the RRL emission, but in those cases it is inconsistent with the RRL emission in spatial location or size and is often associated with other known objects. We therefore do not consider that MIR emission is associated with these nine AVFs, and correspondingly, find no evidence that AVFs are H II regions.

All ten AVF spectra show HI spectrally coincident with the AVF’s RRL emission, which signals the presence of associated neutral gas. Since HI emits at all allowed velocities in the Galaxy, this result is expected. Four AVFs have ^{13}CO spatially coincident with the RRL emission, and six AVF spectra show spectrally coincident ^{13}CO emission. For these six, however, the RRL and ^{13}CO emission have different spatial distributions. While the circle defining the limits of each AVF is drawn to fit as tightly as possible, the AVFs are not circular so the RRL emission does not completely fill the circle. In these six cases, ^{13}CO emission is observed inside the circle over which the spectrum is integrated, but is not spatially coincident with the RRL emission.

Eight AVFs are at least partially co-spatial with objects from the WISE Catalog. Among these eight AVFs, there are 13 known H II regions, 11 H II region candidates, and 12 radio-quiet H II regions fully or partially co-spatial with an AVF. Based on their relative loca-

tions, angular sizes, and velocities we do not consider any of the catalog objects to be associated with the AVFs. In the case of the known H II regions, we check the AVF’s velocity against the velocity of the H II region reported in the WISE Catalog. If they are not within $20\ \text{km s}^{-1}$, we consider the AVF and H II region unlikely to be associated. We also compare the position and morphology of the AVF to the reported size and position of the H II region in the WISE Catalog. In all cases, either the velocity does not match, the position and morphology do not match, or both. We require all these criteria to match in order to consider the AVF and H II region to be associated. H II region candidates and radio-quiet sources do not have measured velocities, and as such, we cannot make a velocity comparison between these regions and the AVFs. The position and morphology of the AVFs do not correspond to any such sources in the WISE Catalog.

In Figure 6 we show the location of these AVFs on a longitude-velocity (LV) diagram along with GDIGS data, and known H II regions from the WISE Catalog. We also show rectangles with the approximate longitude and velocity ranges of Bania’s Clumps 1 and 2 (Bania 1977). These clumps are large, isolated regions of ^{12}CO emission observed in the direction of the inner Galaxy. Both are $\sim 1^\circ$ wide in Galactic longitude, with Clump 1 centered at $\sim 355^\circ$ and Clump 2 centered at $\sim 3^\circ$. Clump 1 spans a velocity range of $\sim 60 - 120\ \text{km s}^{-1}$ while Clump 2 covers a range of $\sim 50 - 150\ \text{km s}^{-1}$. The velocity range of Clump 1 exceeds that allowed by circular rotation at its Galactic longitude, and therefore much of its velocity is expected to be noncircular (Bania 1977). Clump 2 is notable for having the second widest velocity range of all Galactic ^{12}CO features, with only the nuclear disk exceeding it. Bania’s Clumps are observed over longitude and velocity ranges comparable to some of the AVFs, and are included for comparison.

Fig. Set 5. Anomalous Velocity Features (AVFs)

The WISE Catalog contains two known H II regions that also have unusually high velocities: G002.614+00.133, which has a velocity of $102.4\ \text{km s}^{-1}$ (Lockman 1989), and G007.700–00.123, which has a velocity of $151.5\ \text{km s}^{-1}$ (Anderson et al. 2018b). The AVFs may be of a related class. Both of the known H II regions, however, have coincident $24\ \mu\text{m}$ emission, whereas the AVFs lack such emission. Roughly 80% of H II regions have associated ^{13}CO emission (Anderson et al. 2009). Meanwhile, only 6 out of the 10 AVFs’ spectra show ^{13}CO emission at the same velocity as the RRL emission. Only 1 out of the 10 AVFs, G355.612+00.314, shows ^{13}CO spatially associated with the RRL emission,

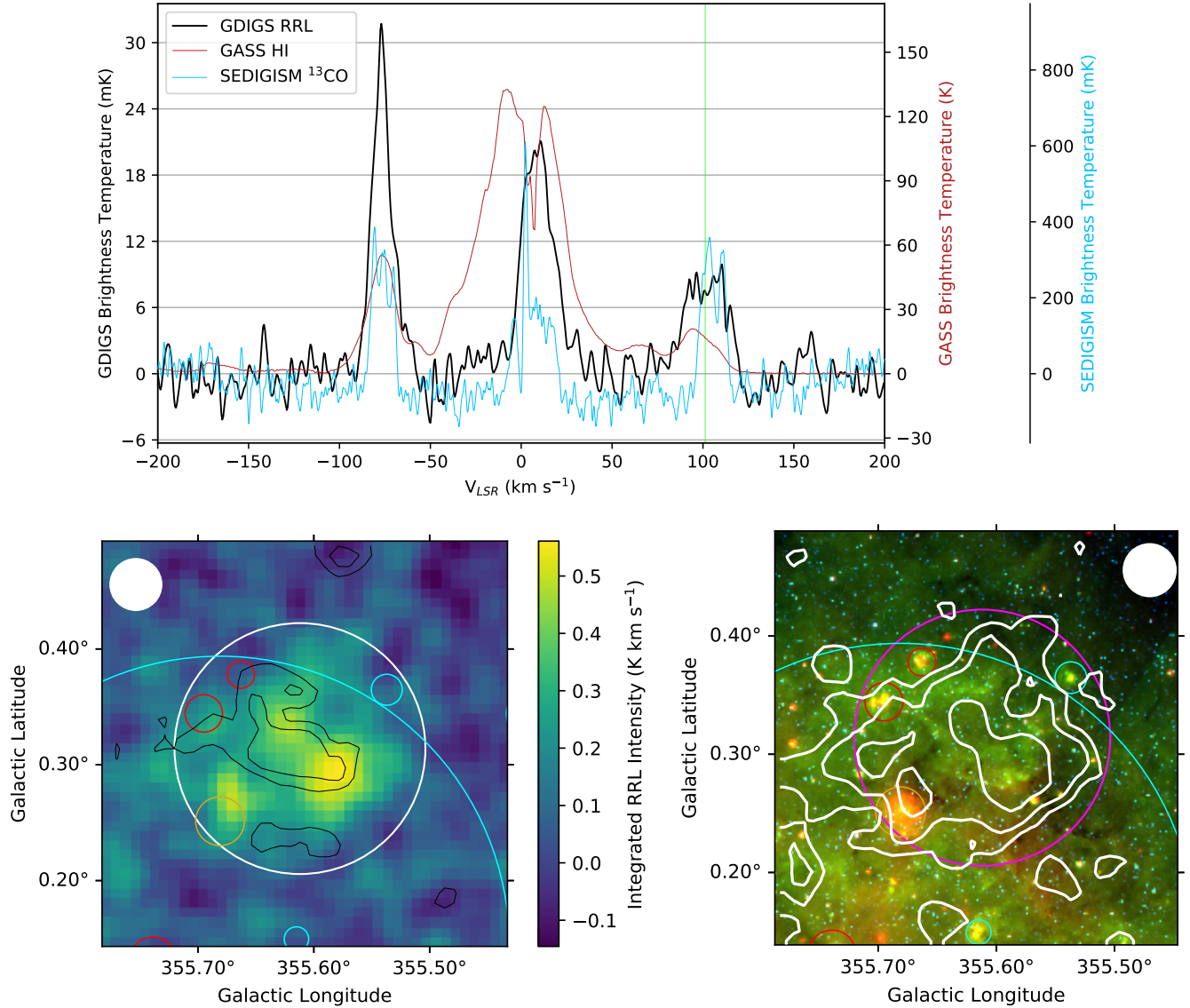


Figure 5. Top: Spectra for AVF G355.612+00.314. GDIGS RRL data are shown in black, GASS HI data in red, and SEDIGISM ^{13}CO data in blue. The GDIGS data are spectrally Gaussian-smoothed with a FWHM of 2.35 km s^{-1} . The vertical green line marks the estimated velocity of the AVF. Bottom left: Moment 0 map for the same AVF. The color map displays the GDIGS RRL Moment 0 integrated intensity, while the black contours display the SEDIGISM ^{13}CO Moment 0 integrated intensity. As in Section 3.1.1, the Moment 0 integration is carried out over a velocity range equal to the FWHM and centered on the LSR velocity. The ^{13}CO data are spatially Gaussian-smoothed with a FWHM of $19''$. The contour levels are at 2σ and 3.5σ , where σ is the standard deviation of the ^{13}CO Moment 0 intensity across the circle. The white circle marks the estimated extent of the AVF. The filled white circle in the upper left shows the $2'.65$ GDIGS beam size. Red circles mark known H II regions, orange circles mark radio-quiet H II regions, and cyan circles mark H II region candidates, all from the WISE Catalog. Of the two known H II regions in the area, the northern one has a velocity of -2.6 km s^{-1} while the other has velocity components of 3.0 km s^{-1} and -79.1 km s^{-1} . We do not think either is associated with the AVF. Bottom right: Example three-color composite image of the same AVF made from Spitzer MIR data; $24 \mu\text{m}$ emission is represented in red, $8 \mu\text{m}$ emission is represented in green, and $3.6 \mu\text{m}$ emission is represented in blue. White contours display the GDIGS RRL Moment 0 intensity from the left panel. The contours on this map are at σ , 1.8σ , and 3.1σ , where σ is the standard deviation of the RRL Moment 0 intensity across the circle. A magenta circle marks the estimated extent of the AVF, and red, orange, and cyan circles mark H II regions, radio-quiet H II regions, and H II region candidates from the WISE catalog. The filled white circle in the upper right again shows the $2'.65$ GDIGS beam size. A figure set containing maps and spectra for the 10 AVFs discussed in Section 3.2.3 is available in the online version of this article.

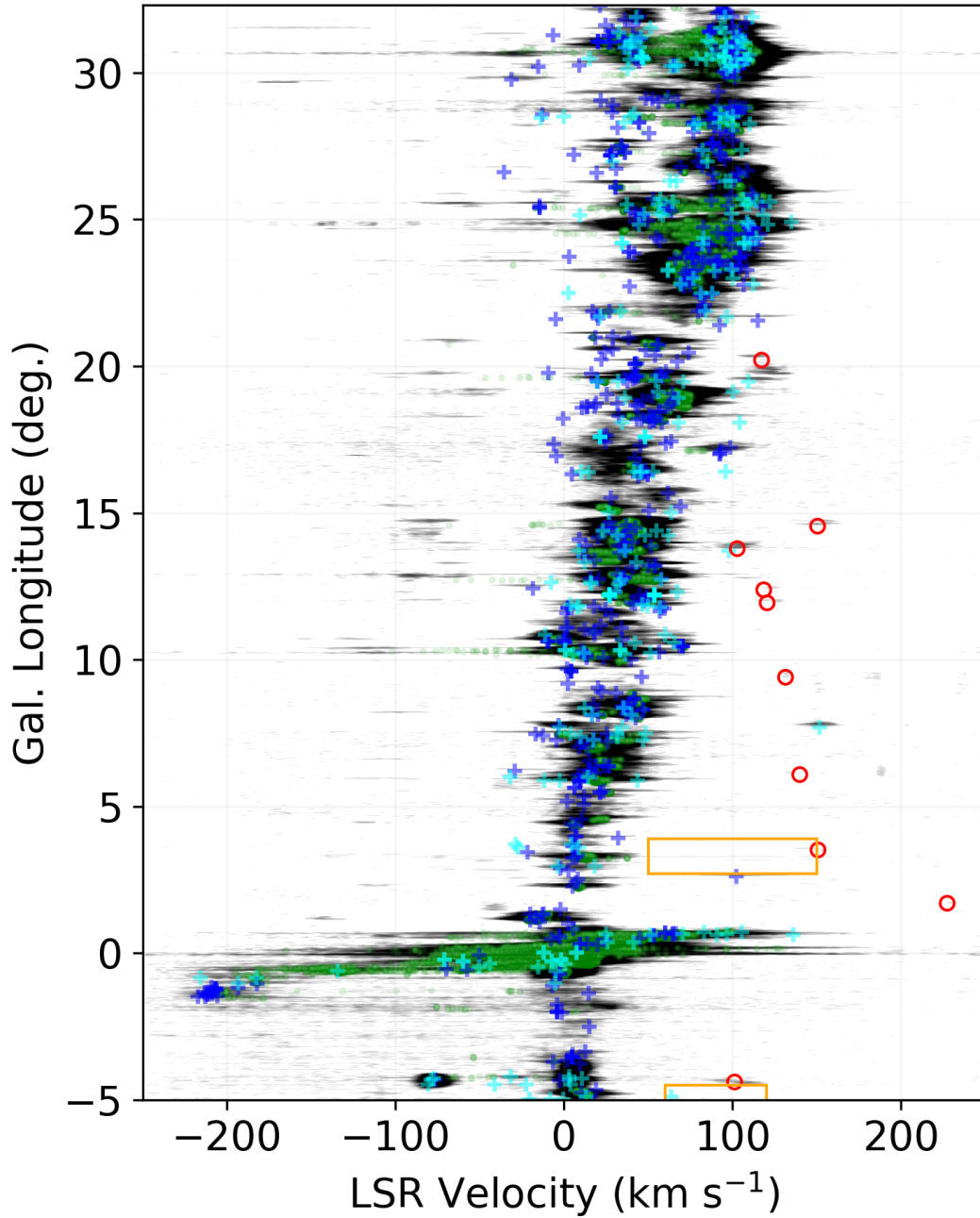


Figure 6. Longitude-velocity (LV) diagram of the GDIGS survey data (grayscale). Known H II regions from the WISE catalog are marked with crosses: blue for regions with one velocity component, cyan for each component of those with multiple velocity components. Small green circles mark the centroids of the Gaussian decompositions of the GDIGS data (see [Anderson et al. 2021](#)). Larger red circles mark the AVFs. The orange boxes show the approximate position and dimensions of Bania's Clump 1 and 2 ([Bania 1977](#)).

and that AVF’s RRL emission is not associated with MIR emission. Based on the lack of ^{13}CO and $24\ \mu\text{m}$ emission from these objects, we consider it unlikely that they are H II regions. To what class of object the AVFs belong remains undetermined.

The LV diagram of RRL emission presented in Hou et al. (2022) shows some compact emission at velocities between 100 and 150 km s^{-1} . These features, however, have very narrow linewidths indicating that they are noise.

Below, we discuss noteworthy features of the most interesting individual AVFs.

- AVF G355.612+00.314 is the only AVF observed in the fourth Galactic quadrant. It is presented as an example in Figure 5 because it demonstrates the aspects of AVFs outlined above: multiple bright areas connected by diffuse emission which completely surrounds them, spatially coincident ^{13}CO emission, $24\ \mu\text{m}$ MIR emission associated with another object, spectrally coincident H I and ^{13}CO emission, and several coincident but unassociated objects from the WISE catalog. This AVF also falls within the velocity range of Bania’s Clump 1, and sits on the edge of the Clump 1 longitude range (Bania 1977), as seen in Figure 6. The AVF may be part of the Clump 1 complex, but according to SEDIGISM $^{13}\text{CO}\ 2-1$ data it is not coincident spatially or spectrally with the bulk of the Clump 1 ^{13}CO emission.
- AVF G001.702–00.156 is the closest in longitude to the Galactic Center and, at +232.0 km s^{-1} , has the highest LSR velocity of all the observed AVFs. Visual inspection of its position on the LV diagram (Figure 6) suggests it may be associated with a Galactic Center structure, likely the nuclear disk. The nuclear disk, also referred to as the nuclear ring or central molecular zone (CMZ), is a zone of high-velocity gas located within the inner ~ 0.5 kpc of the Milky Way (Sormani et al. 2019). We base this inference on the behavior of the known H II regions and the RRL observations near the Galactic center, which roughly form a slanted spike structure on the LV diagram representing the nuclear disk (Fux 1999). A line drawn to continue the apparent structure would pass near this AVF. This AVF’s velocity is outside the velocity range of the ^{13}CO data used here, so no ^{13}CO comparison is made.
- AVF G003.158–00.040 sits at the edge of the velocity range of Bania’s Clump 2 and is within its longitude range (Bania 1977), as seen in

Figure 6. Like G355.612+0.314 and Clump 1, G003.158–0.040 straddles the edge of the box representing the longitude-velocity bounds of Clump 2, and we are likewise unable to conclude whether or not this AVF is associated with the Clump.

- AVF G009.402+00.180 has an exceptionally small FWHM, at only 5.1 km s^{-1} . This value implies a low plasma temperature, an unusually low amount of turbulence, or both.
- AVF G013.782–00.152 is the AVF with the lowest LSR velocity in the first Galactic quadrant, and the second lowest LSR velocity overall after G355.612+00.314. One velocity component of the WISE H II region G013.709–00.243, at 97.8 km s^{-1} , is within 10 km s^{-1} of the AVF’s velocity, but the region is small in size relative to the AVF and it is far from the AVF’s centroid, so we cannot draw any conclusions in regard to a possible association.
- AVF G020.206+00.036 has the greatest Galactic longitude by more than 5° . It is the closest in velocity to the bulk of the H II emission, but is distinct enough to be noticeable on Figure 6. This AVF has a small amount of coincident $24\ \mu\text{m}$ emission, but the morphology does not resemble that expected of an H II region.

4.4. FWHM Analysis

The FWHM line width is related to the thermal and turbulent motions in the plasma. We can compare the trends in the FWHM values between known WISE Catalog objects and newly discovered regions to check for additional differences between the categories. To that end, we calculate the mean and standard deviation of the FWHM line widths for known WISE Catalog regions, including those with first spectroscopic detections reported in this paper, and for each category of newly discovered region. We exclude regions with multiple velocity components. These statistics, as well as the number of included sources in each category, are reported in Table 9. There are too few new H II regions and AVFs to reasonably draw conclusions from their statistics. The mean FWHM of the DEZs is greater than that of the WISE Catalog objects, but is within one standard deviation. We therefore cannot conclude any additional distinctions between the DEZs and WISE Catalog regions from FWHM trends alone.

5. SUMMARY

Table 9. FWHM Line Width Statistics

Source Category	Mean	St. Dev.	Number
	(km s^{-1})	(km s^{-1})	
WISE Catalog Objects	25.1	7.2	2279
New H II Regions	31.7	5.5	4
DEZs	32.2	11.5	21
AVFs	21.5	7.3	10

We use GDIGS RRL data to identify and characterize RRL features from discrete sources of emission. We summarize these results below.

- We identify from the GDIGS data the H II region velocity of 35 sources with multiple previously-reported velocity components. We hypothesize that for H II regions with multiple observed velocities, the velocity or velocities not associated with the H II region itself belong to DIG along the line of sight.
- We detect RRL emission for 40 “group” H II regions, 27 H II region candidates, and 21 radio quiet H II regions, all from the WISE catalog. In total, we move 89 WISE Catalog objects into the “known” H II region category.

- We detect RRL emission from eight locations that we believe to be previously unknown Galactic H II regions.
- We detect 30 GDIGS discrete sources that lack coincident MIR emission, and therefore we conclude they are not H II regions. We detect and characterize via Gaussian fitting the RRL emission from these locations.
- Finally, we identify 10 locations of anomalously high-velocity RRL emission, which we refer to as AVFs. We examine the emission at these locations using ^{13}CO , H I, and MIR data. Based on this analysis we conclude that the AVFs are likely not H II regions. Beyond that, we do not have sufficient information to determine to what class of object they belong.

We present Gaussian fit parameters for 96 H II regions, 30 DEZs, and 10 anomalous velocity features. Of these, the 30 DEZs, the 10 AVFs, and eight of the H II regions were previously unknown; the rest lacked observed RRL spectra. These parameters, specifically the LSR velocities, allow calculation of the kinematic distance to these objects. The kinematic distance in turn allows determination of other physical parameters including physical extent of the regions.

APPENDIX

A. WISE CATALOG

We have updated the WISE Catalog of Galactic H II Regions website¹ with results from these observations. This includes the addition of LSR velocities for 88 H II regions; updated velocities for 39 H II regions with multiple velocity components; and 8 new H II regions.

ACKNOWLEDGMENTS

This work is supported by NSF grant AST1516021 to LDA. The National Radio Astronomy Observatory is a facility of the National Science Foundation operated under cooperative agreement by Associated Universities, Inc. The Green Bank Observatory is a facility of the National Science Foundation operated under cooperative agreement by Associated Universities, Inc. We thank the staff at the Green Bank Observatory for their hospitality and friendship during the observations and data reduction. We thank West Virginia University for its financial support of GBT operations, which enabled some of the observations for this project.

Part of this publication is based on data acquired with the Atacama Pathfinder Experiment (APEX) under programs 092.F-9315 and 193.C-0584. APEX is a collaboration among the Max-Planck-Institut für Radioastronomie, the European Southern Observatory, and the Onsala Space Observatory. The processed data products are available from the SEDIGISM survey database located at <https://sedigism.mpifr-bonn.mpg.de/index.html>, which was constructed by James Urquhart and hosted by the Max Planck Institute for Radio Astronomy.

¹ <http://astro.phys.wvu.edu/wise>

This publication makes use of molecular line data from the Boston University-FCRAO Galactic Ring Survey (GRS). The GRS is a joint project of Boston University and Five College Radio Astronomy Observatory, funded by the National Science Foundation under grants AST-9800334, AST-0098562, AST-0100793, AST-0228993, & AST-0507657.

T.V.W. is supported by a National Science Foundation Astronomy and Astrophysics Postdoctoral Fellowship under award AST-2202340.

Software: AstroPy (Astropy Collaboration et al. 2013; Price-Whelan et al. 2018; Astropy Collaboration et al. 2022)

REFERENCES

- Alves, M. I. R., Calabretta, M., Davies, R. D., et al. 2015, MNRAS, 450, 2025, doi: [10.1093/mnras/stv751](https://doi.org/10.1093/mnras/stv751)
- Anderson, L. D., Armentrout, W. P., Luisi, M., et al. 2018a, ApJS, 234, 33, doi: [10.3847/1538-4365/aa956a](https://doi.org/10.3847/1538-4365/aa956a)
- . 2018b, VizieR Online Data Catalog, J/ApJS/234/33
- Anderson, L. D., & Bania, T. M. 2009, ApJ, 690, 706, doi: [10.1088/0004-637X/690/1/706](https://doi.org/10.1088/0004-637X/690/1/706)
- Anderson, L. D., Bania, T. M., Balser, D. S., et al. 2014, ApJS, 212, 1, doi: [10.1088/0067-0049/212/1/1](https://doi.org/10.1088/0067-0049/212/1/1)
- Anderson, L. D., Bania, T. M., Balser, D. S., & Rood, R. T. 2011a, VizieR Online Data Catalog, J/ApJS/194/32
- . 2011b, ApJS, 194, 32, doi: [10.1088/0067-0049/194/2/32](https://doi.org/10.1088/0067-0049/194/2/32)
- Anderson, L. D., Bania, T. M., Jackson, J. M., et al. 2009, ApJS, 181, 255, doi: [10.1088/0067-0049/181/1/255](https://doi.org/10.1088/0067-0049/181/1/255)
- Anderson, L. D., Hough, L. A., Wenger, T. V., Bania, T. M., & Balser, D. S. 2015a, ApJ, 810, 42, doi: [10.1088/0004-637X/810/1/42](https://doi.org/10.1088/0004-637X/810/1/42)
- Anderson, L. D., Zavagno, A., Barlow, M. J., García-Lario, P., & Noriega-Crespo, A. 2012, A&A, 537, A1, doi: [10.1051/0004-6361/201117640](https://doi.org/10.1051/0004-6361/201117640)
- Anderson, L. D., Deharveng, L., Zavagno, A., et al. 2015b, ApJ, 800, 101, doi: [10.1088/0004-637X/800/2/101](https://doi.org/10.1088/0004-637X/800/2/101)
- . 2015c, ApJ, 800, 101, doi: [10.1088/0004-637X/800/2/101](https://doi.org/10.1088/0004-637X/800/2/101)
- Anderson, L. D., Luisi, M., Liu, B., et al. 2021, ApJS, 254, 28, doi: [10.3847/1538-4365/abef65](https://doi.org/10.3847/1538-4365/abef65)
- Armentrout, W. P., Anderson, L. D., Balser, D. S., et al. 2017, ApJ, 841, 121, doi: [10.3847/1538-4357/aa71a1](https://doi.org/10.3847/1538-4357/aa71a1)
- Astropy Collaboration, Robitaille, T. P., Tollerud, E. J., et al. 2013, A&A, 558, A33, doi: [10.1051/0004-6361/201322068](https://doi.org/10.1051/0004-6361/201322068)
- Astropy Collaboration, Price-Whelan, A. M., Lim, P. L., et al. 2022, ApJ, 935, 167, doi: [10.3847/1538-4357/ac7c74](https://doi.org/10.3847/1538-4357/ac7c74)
- Bania, T. M. 1977, ApJ, 216, 381, doi: [10.1086/155478](https://doi.org/10.1086/155478)
- Benjamin, R. A., Churchwell, E., Babler, B. L., et al. 2003, PASP, 115, 953, doi: [10.1086/376696](https://doi.org/10.1086/376696)
- Carey, S. J., Noriega-Crespo, A., Mizuno, D. R., et al. 2009, PASP, 121, 76, doi: [10.1086/596581](https://doi.org/10.1086/596581)
- Churchwell, E., Babler, B. L., Meade, M. R., et al. 2009, PASP, 121, 213, doi: [10.1086/597811](https://doi.org/10.1086/597811)
- Fuerst, E., Reich, W., & Sofue, Y. 1987, A&AS, 71, 63
- Fux, R. 1999, A&A, 345, 787, <https://arxiv.org/abs/astro-ph/9903154>
- Haffner, L. M., Reynolds, R. J., Tufte, S. L., et al. 2003, ApJS, 149, 405, doi: [10.1086/378850](https://doi.org/10.1086/378850)
- Hou, L., Han, J., Hong, T., Gao, X., & Wang, C. 2022, Science China Physics, Mechanics, and Astronomy, 65, 129703, doi: [10.1007/s11433-022-2039-8](https://doi.org/10.1007/s11433-022-2039-8)
- Jackson, J. M., Rathborne, J. M., Shah, R. Y., et al. 2006, ApJS, 163, 145, doi: [10.1086/500091](https://doi.org/10.1086/500091)
- Lenz, D. D., & Ayres, T. R. 1992, PASP, 104, 1104, doi: [10.1086/133096](https://doi.org/10.1086/133096)
- Liu, B., Anderson, L. D., McIntyre, T., et al. 2019, The Astrophysical Journal Supplement Series, 240, 14, doi: [10.3847/1538-4365/aaef8e](https://doi.org/10.3847/1538-4365/aaef8e)
- Liu, B., McIntyre, T., Terzian, Y., et al. 2013, AJ, 146, 80, doi: [10.1088/0004-6256/146/4/80](https://doi.org/10.1088/0004-6256/146/4/80)
- Lockman, F. J. 1989, ApJS, 71, 469, doi: [10.1086/191383](https://doi.org/10.1086/191383)
- Lockman, F. J., & Brown, R. L. 1975, ApJ, 201, 134, doi: [10.1086/153867](https://doi.org/10.1086/153867)
- Lyne, A. G., Manchester, R. N., & Taylor, J. H. 1985, MNRAS, 213, 613, doi: [10.1093/mnras/213.3.613](https://doi.org/10.1093/mnras/213.3.613)
- McClure-Griffiths, N. M., Pisano, D. J., Calabretta, M. R., et al. 2009, The Astrophysical Journal Supplement Series, 181, 398–412, doi: [10.1088/0067-0049/181/2/398](https://doi.org/10.1088/0067-0049/181/2/398)
- Price-Whelan, A. M., Sipőcz, B. M., Günther, H. M., et al. 2018, AJ, 156, 123, doi: [10.3847/1538-3881/aabc4f](https://doi.org/10.3847/1538-3881/aabc4f)
- Reid, M. J., Menten, K. M., Brunthaler, A., et al. 2019, ApJ, 885, 131, doi: [10.3847/1538-4357/ab4a11](https://doi.org/10.3847/1538-4357/ab4a11)
- Reynolds, R. J. 1991, in IAU Symposium, Vol. 144, The Interstellar Disk-Halo Connection in Galaxies, ed. H. Bloemen, 67–76
- Reynolds, R. J., Tufte, S. L., Haffner, L. M., Jaehnig, K., & Percival, J. W. 1998, PASA, 15, 14, doi: [10.1071/AS98014](https://doi.org/10.1071/AS98014)
- Schuller, F., Urquhart, J. S., Csengeri, T., et al. 2020, Monthly Notices of the Royal Astronomical Society, 500, 3064–3082, doi: [10.1093/mnras/staa2369](https://doi.org/10.1093/mnras/staa2369)
- Sormani, M. C., Treß, R. G., Glover, S. C. O., et al. 2019, MNRAS, 488, 4663, doi: [10.1093/mnras/stz2054](https://doi.org/10.1093/mnras/stz2054)
- Wenger, T. V., Dawson, J. R., Dickey, J. M., et al. 2021, ApJS, 254, 36, doi: [10.3847/1538-4365/abf4d4](https://doi.org/10.3847/1538-4365/abf4d4)